ONE-SHOT THREE-DIMENSIONAL SURFACE PROFILOMETRY USING DMD-BASED TWO-FREQUENCY MOIRÉ AND FOURIER TRANSFORM TECHNIQUE

L. C. Chen[1], C. H. Cho and X. L. Nguyen
Graduate Institute of Automation Technology,
National Taipei University of Technology, Taipei 106, Taiwan
Email: lcchen@ntut.edu.tw[1]

Abstract- This article presents an optical measurement method for acquiring rapidly accurate geometric 3-D surface morphology of objects. To achieve high-speed profilometry and avoid disturbance due to in-field vibration, one-shot Fourier transform profilometry (FTP) using two-wavelength digital moiré pattern was developed to detect the morphology of the measured object at a speed of up to 60 frames or more per second. Single-fringe interferogram sufficient for FTP can be rapidly captured within a theoretical CCD acquisition time of down to 1 μs. The interferogram thus captured can be applied for further phase retrieving using the developed frequency transform and band-pass filtering strategies. The band-pass filter is designed to obtain phase information for optimizing the 3-D surface reconstruction with both dimensional and structural measurement accuracy. Furthermore, a standard step-height target was measured to analyze accuracy and repeatability of the developed methodology. Experimental results verified that the measurable step height can be effectively increased using the equivalent wavelength established by analyzing two-frequency moiré pattern, thus increasing practical applicability of the developed system while achieving a micro-scale measuring depth resolution. The maximum measured error can be kept within 3.5% of the overall measuring range.

Index terms*:* Optical metrology, Automatic optical inspection (AOI), Fourier transform, Surface profilometry, Fourier transform profilometry (FTP), Dynamic measurement.

I. INTRODUCTION

3-D surface profilometry has become extremely important for high-tech manufacturing industries with applications in modern fields such as nanotechnology, biotechnology, broadband

communication, and optoelectronics. In such applications, a considerable amount of research and development work has been performed to increase the performances of 3-D measurement systems using automatic optical inspection (AOI) techniques. One of the current significant issues in obtaining accurate dimensional information is dealing with anti-vibration problems encountered in on-line inspection environment. How to avoid employing expensive anti-vibration facilities or taking strict operation requirements in in-field 3-D measurement has thus become a critical problem to tackle.

Among currently used methods, interferometry, confocal measurement and moiré fringe projection are the most popular approaches employed for out-of-plane surface profilometry. Interferometry is capable of providing the highest resolution on surface profilometry with nano-scale repeatability [1,2]. Conventional interferometry evaluates the interference of two light waves being reflected on a reference surface and the object to be profiled. However, difficulties in satisfying the requirements either for real-time measurement requirements or for overcoming environmental vibration and disturbance cannot be overcome in many practical applications. Confocal measurement utilized as a surface profilometer has its exclusive advantages in possessing high longitudinal depth resolution and non-contact scanning property. The confocal principle employs two conjugate focal points geometrically matched to both the object surface and the point detector defined by a pinhole aperture. The object is scanned through the focal point and the peak intensity can be detected only when the focal point lies directly on the surface of the sample. However, this approach does not address a key issue encountered in on-line process inspection, in which the vertical scanning time involved in confocal measurement cannot meet the real-time measurement required by many automatic optical inspection (AOI) industries [3].

Another well-developed method involves projecting fringes onto the object using the computerized liquid-crystal-display (LCD) or digital micromirror device (DMD) projection method [4,5]. Digital fringe projection (DFP) is capable of generating concurrently arbitrary fringe patterns of different wavelengths. For DFP, phase shifting profilometry (PSP) and Fourier transform profilometry (FTP) are two of the most important algorithms for 3-D surface contouring [6,7,8,9]. The PSP method generally requires at least three phase shifting interferograms for performing phase wrapping and unwrapping, with one constraint that any adjacent detecting pixel is within $\lambda/4$ phase difference. The FTP method has the advantage of

requiring only one interferogram to establish 3-D profile of the measured object. However, the measurement accuracy achieved is, in general, less than that obtained by the PSP method due to its lower signal-to-noise ratios. Although the FTP method using single-frequency moiré fringe has been established previously [10], the issue of achieving both a high step-height measurement range and a high vertical resolution simultaneously remains unresolved. Nevertheless, for the traditional methods currently employed, the measurement speed and accuracy may pose problems to their applications in in-field 3-D measurement.

To address the above issues, this research proposes an optical measurement method for acquiring rapidly accurate geometric 3-D surface morphology using DMD-based two-frequency moiré and Fourier transform technique. To achieve high-speed profilometry and minimize disturbance due to in-field vibration, fast Fourier transform profilometry (FTP) using two-wavelength digital moiré was developed to detect the morphology of the measured object at a speed of more than 60 fps. In addition, to increase the step-height measurement range, two-wavelength digital moiré was developed to overcome the limits of $\lambda/4$ phase difference between neighboring pixels. Most importantly, a band-pass filter was designed to optimize the 3-D surface reconstruction with both dimensional and form measurement accuracy.

This article comprising six sections is organized as follows. After the introduction above, Section 2 provides a literature review on various types of high-speed 3-D surface profilometry. Following this, the principle of the proposed measurement method is detailed in Section 3. To achieve high-speed image acquisition of the deformed moiré fringe from the object surface. Section 4 describes the system layout of the developed optical measurement system with its design of strobed LED light source and signal synchronizing electronics. With the experimental results, Section 5 illustrates and analyzes the performances of the developed methods from surface measurement on precision gauge blocks and dynamic vibratory characterization of a sound vibratory membrane. Section 6 summarizes the development and the achievements.

II. LITERATURE REVIEW

There are generally three kinds of algorithms used for high speed 3-D surface profilometry involving moiré fringe projection. They are phase shifting, color-encoded structured light and Fourier transform filtering. Stroboscopic imaging is important for acquiring high contrast images

from dynamic objects. The latest development trend as well as the important characteristics of these methods is discussed in the following.

a. Phase shifting methods

Traditional phase shifting generally requires at least three phase shifting interferograms for performing phase wrapping and unwrapping, with one constraint that any adjacent detecting pixel should be within$\lambda/4$ phase difference. To achieve rapid surface profilometry, Zhang presented fast phase shifting employing a high-speed CCD at a frequency of 240 Hz to acquire a series of deformed fringe images according to the DMD projection principle [11]. The method is still limited in measurement bandwidth because at least three different phase fringe patterns are required for each surface frame reconstruction. To achieve simultaneous phase shifting, Wyant developed an optical layout using polarizing masks and beam splitters to obtain four phase maps simultaneously [12]. However, the method could still be hindered by the size of its measurable step height. In addition, the field of view (FOV) of Wyrant's method is decreased to a quarter of the original size.

b. Color-encoded structured light methods

Surface profilometry can be realized by projecting a coded sequence of structure fringes onto the object. Identifying each deformed pattern highlights its original undistorted position to allow calculation of the 3-D depth. The most difficult task encountered by the color-encoded method is accurate detection of the correspondence between the original and deformed patterns. A single binary encoded pattern obtained from De Bruijn sequences was suggested to resolve the issue, in which a unique pattern structure formed by 63 gray stripes was designed for robust recognition [13]. To improve the spatial resolution of the measurement, Griffin proposed a pseudorandom array for encoding a unique structured pattern [14]. Hall-Holt also presented a coded technique by coding the boundaries between stripes for improving measurement accuracy [15]. Owing to complexity in optical occlusion and light variance in real-world measurement environment, the color-encoded structured light methods tend to be complicated and time-consuming for decoding the deformed patterns. Moreover, the methods have poorer spatial resolution due to the detection limits of projection fringes caused by both the projector and sensing devices.

c. Fourier transform filtering methods

Requiring only one interferogram to establish 3-D profile of the measured object, FTP was first proposed by Takeda in 1983 [16]. In recent years, vibratory shapes like drumhead, speakers and balloon have been achieved using FTP. To speed up the reconstruction, a phase unwrapping algorithm requiring only the first frame wrapped phase was developed to unwrap the phase according to the reasonable assumption that the incremental phase difference between frames should be less than 2p. The stroboscopic imaging techniques have been employed to acquire high contrast images from a vibrating object [17,18]. To increase the measurable step height, a two-wavelength interferometry consisting a YAG and a He-Ne laser was developed using FTP [19]. However, the measurement accuracy could deteriorate due to larger synthetic wavelength. In addition, the measurement accuracy achieved by FTP is generally less than that obtained by the phase shifting method due to its lower signal-to-noise ratios. This article thus proposes a FTP-based two-frequency moiré projection method to address the above issues.

III. MEASUREMENT PRINCIPLE

a. Principle of two-frequency moiré FTP

The FTP using two-frequency digital fringe pattern is described as follows. In the two-frequency digital moiré pattern formed by superposing two single-frequency fringe patterns, there normally exist three fringe elements, including the two single-frequency fringes and the equivalent (moiré) fringe being generated by superimposing the two linear patterns simultaneously. In the approach, two fringe patterns with different spatial frequencies are designed and created by a personal computer (PC). The two fringe patterns are then projected simultaneously by a digital light projection (DLP) system onto the measured object through optical lenses for obtaining desired field of view (FOV) and depth of field (DOF). Following this, a CCD camera is employed to capture a series of images of the deformed fringe from the object. A series of deformed fringe images can be expressed as follows:

$$I(x,y) = a(x,y) + b_1(x,y)\cos[\Phi_1(x,y)] + b_2(x,y)\cos[\Phi_2(x,y)] + b_3(x,y)\cos[\Phi_3(x,y)] \quad (1)$$

where $a(x,y)$ is the average background intensity, $b_n(x,y)$ is the intensity modulation (n = 1, 2, 3), $\Phi_n(x,y)$ denotes the phases (n = 1, 2, 3). The phases $\Phi_n(x,y)$ can be further divided into

carried phases ($\phi_\alpha(x,y)$, $\phi_\beta(x,y)$, $\phi_\gamma(x,y)$) and initial phases ($\phi_1(x,y)$, $\phi_2(x,y)$, $\phi_3(x,y)$) as follows:

$$\begin{cases} \Phi_1(x,y) = \phi_\alpha(x,y) + \phi_1(x,y) \\ \Phi_2(x,y) = \phi_\beta(x,y) + \phi_2(x,y) \\ \Phi_3(x,y) = \phi_\gamma(x,y) + \phi_3(x,y) \end{cases} \tag{2}$$

In Eq. (2), $\phi_\alpha(x,y)$, $\phi_\beta(x,y)$ and $\phi_\gamma(x,y)$ can be expressed by the carried frequencies as follows:

$$\begin{cases} \phi_\alpha = 2\pi(f_{1x}x + f_{1y}y) \\ \phi_\beta = 2\pi(f_{2x}x + f_{2y}y) \\ \phi_\gamma = 2\pi(f_{3x}x + f_{3y}y) \end{cases} \tag{3}$$

where f_{nx} and f_{ny} are the carried frequencies along the x- and y-coordinate of the fringe pattern 1, fringe pattern 2 and equivalent fringe pattern, respectively (n = 1, 2, 3).

From (2), Eq. (1) can be further rewritten as follows:

$$\begin{aligned} i(x,y) = a(x,y) + b_1(x,y)\cos[\phi_\alpha(x,y) + \phi_1(x,y)] \\ + b_2(x,y)\cos[\phi_\beta(x,y) + \phi_2(x,y)] + b_3(x,y)\cos[\phi_\gamma(x,y) + \phi_3(x,y)] \end{aligned} \tag{4}$$

A series of deformed patterns described by Eq. (4) can be rewritten in the following form:

$$\begin{aligned} i(x,y) = a(x,y) + \frac{1}{2}b_1(x,y)\exp[j\phi_1(x,y)]\exp[j\phi_\alpha(x,y)] \\ + \frac{1}{2}b_1(x,y)\exp[-j\phi_1(x,y)]\exp[-j\phi_\alpha(x,y)] \\ + \frac{1}{2}b_2(x,y)\exp[j\phi_2(x,y)]\exp[j\phi_\beta(x,y)] \\ + \frac{1}{2}b_2(x,y)\exp[-j\phi_2(x,y)]\exp[-j\phi_\beta(x,y)] \\ + \frac{1}{2}b_3(x,y)\exp[j\phi_3(x,y)]\exp[j\phi_\gamma(x,y)] \\ + \frac{1}{2}b_3(x,y)\exp[-j\phi_3(x,y)]\exp[-j\phi_\gamma(x,y)] \end{aligned} \tag{5}$$

Equation (5) can be further simplified as:

$$\begin{aligned} i(x,y) = a(x,y) &+ c_1(x,y)\exp[j\phi_\alpha(x,y)] + c_1^*(x,y)\exp[-j\phi_\alpha(x,y)] \\ &+ c_2(x,y)\exp[j\phi_\beta(x,y)] + c_2^*(x,y)\exp[-j\phi_\beta(x,y)] \\ &+ c_3(x,y)\exp[j\phi_\gamma(x,y)] + c_3^*(x,y)\exp[-j\phi_\gamma(x,y)] \end{aligned} \quad (6)$$

where $c_n(x,y) = \frac{1}{2} b_n(x,y)\exp[j\phi_n(x,y)]$.

By using Fourier transform and regarding to Eq. (3), Eq. (6) can be transformed and expressed as:

$$\begin{aligned} I(f_x,f_y) = A(f_x,f_y) &+ C_1(f_x - f_{1x}, f_y - f_{1y}) + C_1^*(f_x + f_{1x}, f_y + f_{1y}) \\ &+ C_2(f_x - f_{2x}, f_y - f_{2y}) + C_2^*(f_x + f_{2x}, f_y + f_{2y}) \\ &+ C_{eq}(f_x - f_{3x}, f_y - f_{3y}) + C_{eq}^*(f_x + f_{3x}, f_y + f_{3y}) \end{aligned} \quad (7)$$

In the proposed method, C_1, C_2 and C_{eq} are equally selected by a band-pass filter and are transformed into the space domain by the inverse Fourier transform, respectively. Furthermore, the height of the 3-D profile can be found in the phase map obtained by phase unwrapping.

b. Strategies for spectrum separation

In FTP, it is important to extract precisely the corresponding spectrum region transformed from the deformed fringe pattern by Fast Fourier Transform (FFT), in order to establish the phase map for accurate surface reconstruction. Because the spectrum data representing patterns of different frequencies may overlap when their carrier-frequency regions are lying too close within the spectrum domain, it could be difficult to extract the whole spectrum region for phase reconstruction. Thus, an effective strategy for ensuring success in spectrum extraction is especially important for two-frequency fringe pattern projection since four spectrum regions representing the background image (dc spectrum portion), the equivalent fringe pattern, the fringe of carrier-frequency 1 and the fringe of carrier-frequency 2 could easily overlap. Any overlapping between spectrum regions could make clear separation of spectrum data difficult and result in inaccurate surface reconstruction.

Figure 1 displays the relationship between the spatial pattern and frequency-domain data of single-frequency and two-frequency linear patterns. When projecting onto a flat surface, a single-frequency pattern with a carrier frequency C_1 can be acquired by the CCD. By using FFT, its spectrum diagram having two spectral peaks representing a background image (dc spectrum portion) and a single carrier-frequency pattern can be obtained as shown in figure 1(a). Similarly, another single-frequency pattern with a carrier frequency C_2 ($C_2 > C_1$) can be transformed to its spectrum domain having a higher spectral peak representing its carrier-frequency (shown in figure 1(b)). Superposing (a) and (b) forms a moiré pattern (shown in figure 1(c)) with its spectrum diagram comprising four spectrum regions, which represent the background image (dc spectrum region, dc), the equivalent fringe pattern, the carrier-frequency 1 and 2 fringe patterns. In general, since the spectral data (C_{eq}) representing the equivalent pattern are normally close to the position of dc spectrum portion, these two regions could easily overlap and C_{eq} is in general difficult to observe or detect. Moreover, if r represents the radius of each spectrum region, clear separation of the three spectrum data regions, including dc, C_1, and C_2, could be achieved only when (C_2- r) is larger than (C_1 + r) and (C_1 - r) is larger than (dc + r).

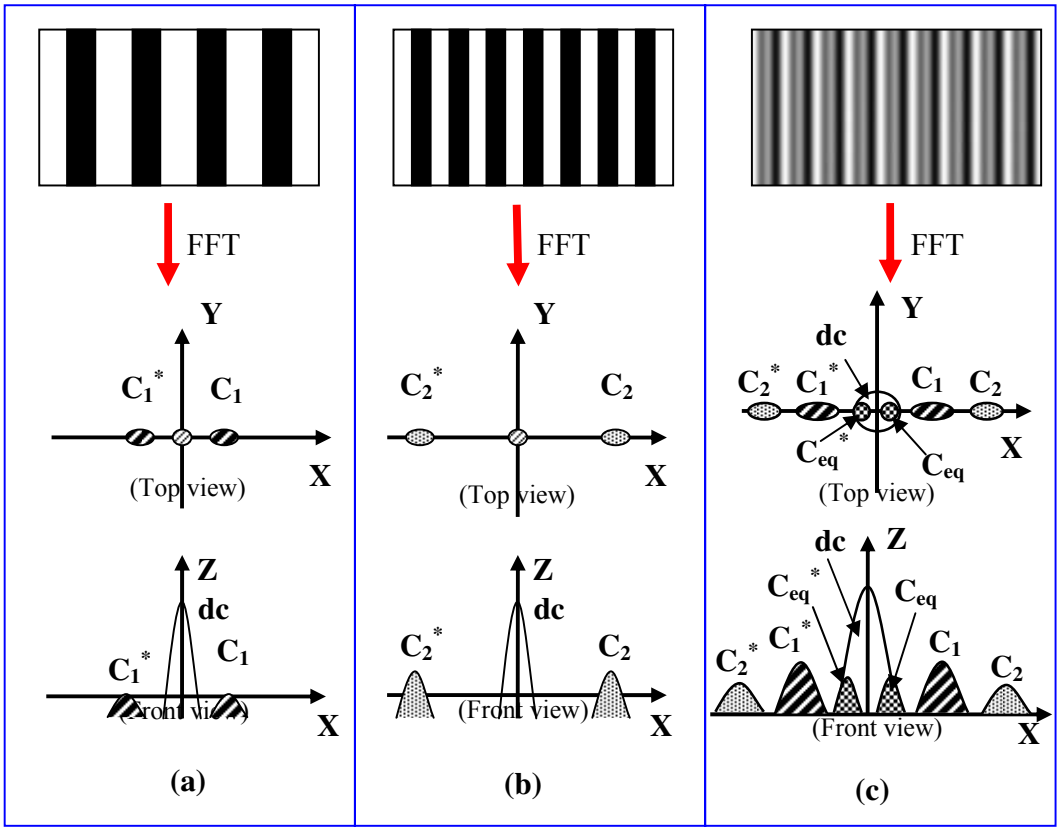

Figure 1. Relationship between spatial pattern and frequency-domain data of single-frequency and two-frequency fringe patterns: (a) a single-frequency fringe with a carrier frequency of C_1; (b) a single-frequency fringe with a carrier frequency of C_2; and (c) a two-frequency fringe fringe with carrier frequencies of C_1,C_2 and C_{eq}.

The relationship between the phase difference $\Delta\phi$ and the carrier frequency (f_0) of the deformed fringe pattern projected onto the object surface can be expressed by Eq. (8).

$$f_0 = \frac{\Delta\phi}{2\pi} \tag{8}$$

It is apparent that f_0 is proportional to $\Delta\phi$. This indicates that the number of fringes in the projected pattern will increase when the phase difference at any adjacent pixel increases. Thus, the surface curvature of the object can influence the size of the spectral data region. When the surface of the measured object is relatively flat, the size of the spectral data region covers a relatively small region. The three frequency components can be easily separated since each spectral region is confined within a relatively small region, as shown in figure 2(a). Accordingly, a band-pass filter can easily separate each spectral region to obtain the phase information. However, because the object surface can be of arbitrary type, such as free-form (continuous) or step-height (discontinuous) surfaces, the size of the spectral data region could increase undesirably to overlap each other, as shown in figure 2(b). In such case, difficulty may arise in the band-pass filtering for ensuring clear spectral data extraction.

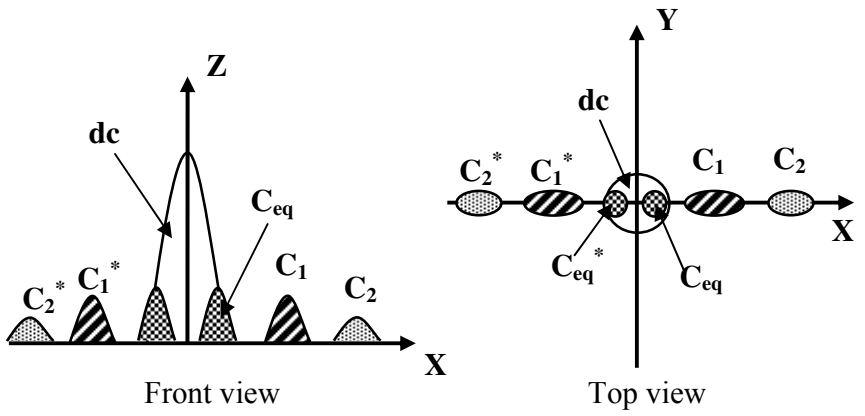

(a)

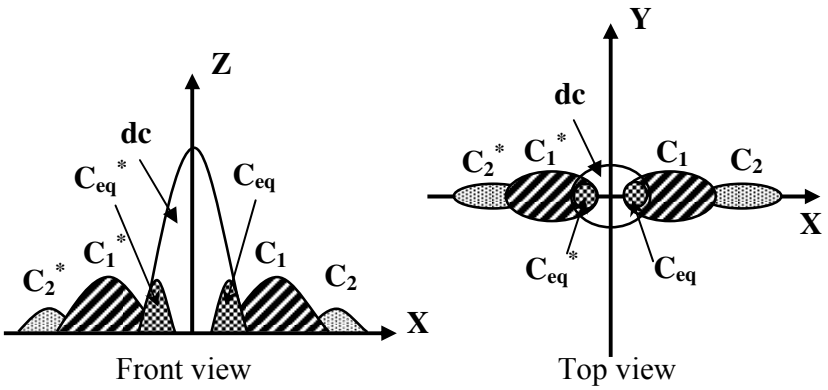

(b)

Figure 2. Distribution of spectral data regions: (a) the spectral data regions are separable when the spectral data region is confined within a reasonable size; and (b) the spectral data regions are overlapped when the spectral data region exceeds a desired size.

To overcome the above problem, two strategies are proposed for ensuring clear spectral data extraction in the two-frequency fringe pattern projection method. The first strategy is proposed to reduce the size of dc spectral region by subtracting the background image from the deformed fringe image. The background image (I_B) is initially acquired before projecting any fringe pattern onto the object to be measured. Following this, by projecting the two-frequency fringe pattern onto the object, the deformed fringe image (I) is then captured. To reduce the dc spectral data, the deformed fringe image is subtracted from the background image as follows:

$$I' = I - I_B \tag{9}$$

Figure 3 illustrates an example for demonstrating the reduction of dc spectral data using the proposed strategy. A two-frequency pattern (P_1 = 5 mm and P_2 = 10 mm) was projected onto a spherical ball with a diameter of 2.0 mm, in which P_1 is the period of the spatial frequency 1, and P_2 is the period of the spatial frequency 2. It is apparent that the dc spectral data can be effectively reduced and the overlapping problem between the dc spectral data and the spectral region 1 can be minimized.

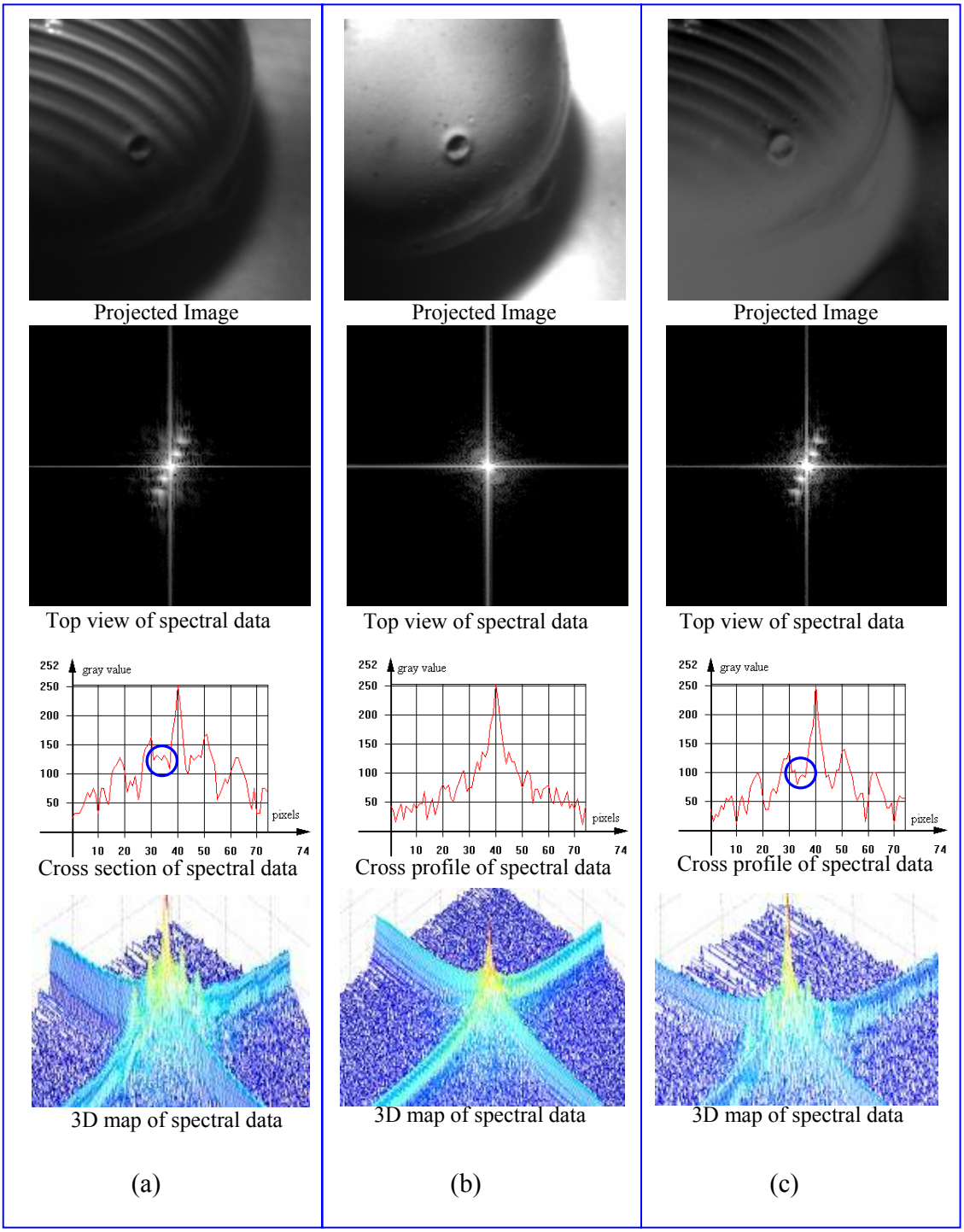

Figure 3. An example demonstrating reduction of dc spectral data using the proposed strategy: (a) the deformed fringe image and its spectrum data (top view, cross section and 3-d view) when projecting a two-frequency sinusoidal moiré fringe onto a spherical ball; (b) the background

image and its spectrum data (top view, cross section and 3-d view); and (c) the net image and its spectrum data obtained (top view, cross section and 3-d view) using the dc reduction strategy.

Although the above strategy may be effective in separating the dc region from the spectral region 1, the overlapping problem between the spectral regions of frequency 1 and 2 still affects the quality of the band-pass filtering. Moreover, the equivalent region (C_{eq}) could be still overlapped with the dc region. Therefore, the second strategy is proposed to separate these spectral regions by designing a two-frequency fringe pattern. Theoretically, the central distance between the spectral peaks 1 and 2 could reach a maximum when the angle between the orientations of two fringes equals 90°. However, because two linear fringe patterns will become mutually independent under this condition, the equivalent wavelength of moiré pattern is ill defined. To achieve both a clear spectrum separation between the spectral data regions and a reasonably large equivalent pattern period for ensuing a reasonable step-height measuring range, a two-frequency fringe pattern with an inclined angle of 45° can be employed for FTP. The equivalent period (P_{eq}) of moiré pattern with an inclined angle of θ between two set of single-frequency patterns can be expressed as:

$$P_{eq} = \frac{P_1 P_2}{\sqrt{P_1^2 + P_2^2 - 2P_1 P_2 \cos\theta}} \tag{10}$$

where P_1 is the period of the fringe pattern 1, P_2 is the period of the fringe pattern 2, and θ is the angle between the orientations of these patterns.

Figure 4 shows an example of a two-frequency pattern by superposing the fringe pattern 1 having a period of 7.5 mm with a 45°-tilting angle and the fringe pattern 2 having a period of 15 mm with a horizontal orientation. The general spectrum diagram of the proposed two-frequency pattern is shown in Figure 5. The advantage of the developed pattern especially in clear separation of C_1, C_2, C_{eq} and dc spectral regions is obvious. In particular, C_{eq} can be clearly separated from the dc region, which cannot be accomplished by a general two-frequency pattern as demonstrated in figure 1. For example, projecting the designed pattern onto a spherical ball yields a deformed fringe pattern shown in figure 6 (a). Using FFT, the spectral region 1, spectral region 2 and the equivalent spectral region can be obtained as shown in figure 6 (b) and (c). It is clear that the three spectral data regions are clearly separated with a reasonable distance in

between. More importantly, C_{eq} can also be clearly separated from the dc spectral region. In this case, the equivalent period of the moiré pattern is 10.58 mm when the period 1 and period 2 of two linear fringe patterns are 7.5 mm and 15 mm, respectively.

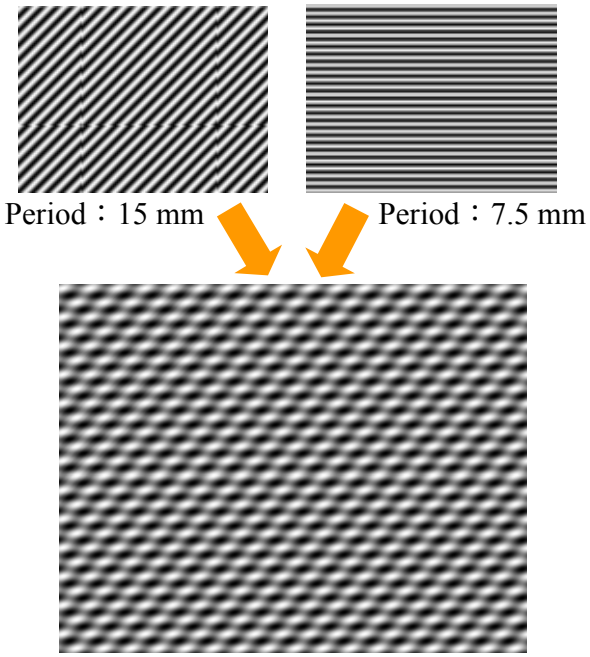

Figure 4. Generation of a two-frequency moiré fringe by superposing the fringe pattern 1 having a period of 15 mm with a 45 ^{o}-tilting angle and the fringe pattern 2 having a period of 7.5 mm with a horizontal orientation.

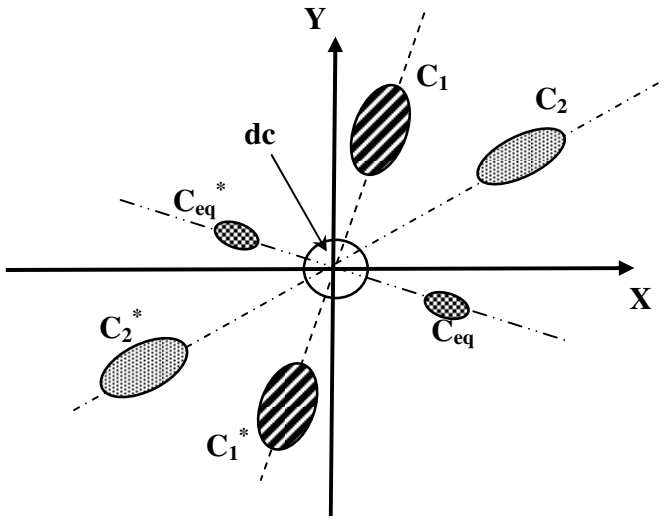

Figure 5. Distribution of spectral data regions of the proposed two-frequency moiré fringe.

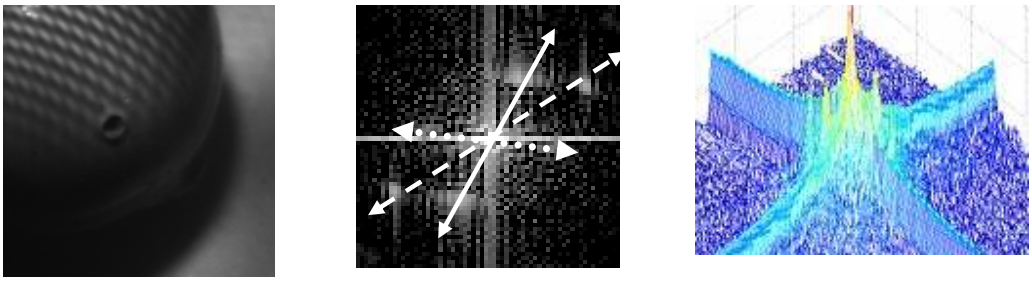

(a) Grabbed image (b) Spectrum data (2D) (c) Spectrum data (3D)

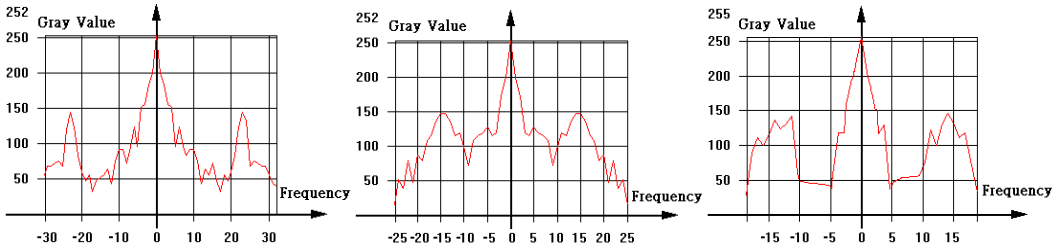

(d) the spectral profile of the fringe pattern 2 (the dashed line in (b))

(e) the spectral profile of the fringe pattern 1(the solid line in (b))

(f) the spectral profile of the equivalent fringe pattern(the dot line in (b))

Figure 6. An example demonstrating spectrum separation when projecting the designed two-frequency sinusoidal moiré fringe onto a spherical ball: (a) the deformed fringe image; (b) the 2-D spectrum data; (c) the 3-D spectrum data; (d) the 2D spectral profile of the fringe pattern 2 along the dashed line in (b); and (e) the 2-D spectral profile of the fringe pattern 1 along the solid line in (b) ; and (f) the 2-D spectral profile of the equivalent (moiré) fringe pattern along the dot line in (b).

Although the above method can generally achieve a clear spectrum separation, the equivalent period of the moiré pattern is sometimes reduced to be even smaller than the period of single pattern. As a result, the maximum measurable step heights cannot be effectively increased. To overcome this drawback, the tilting angle and the period of two spatial frequencies are analyzed to determine the possible maximum equivalent (synthetic) period. According to Eq. (10), the ratio of the period of the fringe pattern 2 with respect to the fringe period 1 is shown in figure 7. Generally, the period of the fringe pattern 2 should be adjusted according to the tilting angle, in

order to achieve a maximum equivalent period. Shown in figure 8, the maximum ratio of the equivalent period with respect to the fringe pattern 1 can be determined according to the tilting angle and the fringe period 2 as defined in figure 7. Theoretically, the equivalent period of the two-frequency moiré pattern can be maximized to become infinite. However, when the tilting angle is decreased, the spectral data regions of the frequency 1 and 2 will overlap. Moreover, the measurement depth resolution is determined by the equivalent period of the pattern, in which the smaller the period is, the higher the resolution becomes. The equivalent period is limited by the image quality index of the optical system, such as modulation transfer function (MTF).

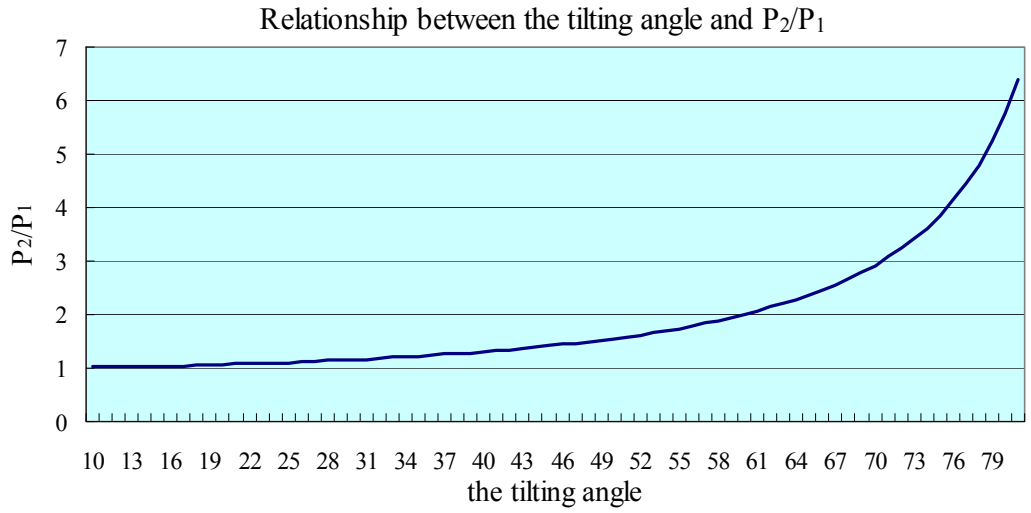

Figure 7. Ratio of fringe period 2 with respect to fringe period 1 determined by tilting angle to achieve maximum equivalent period.

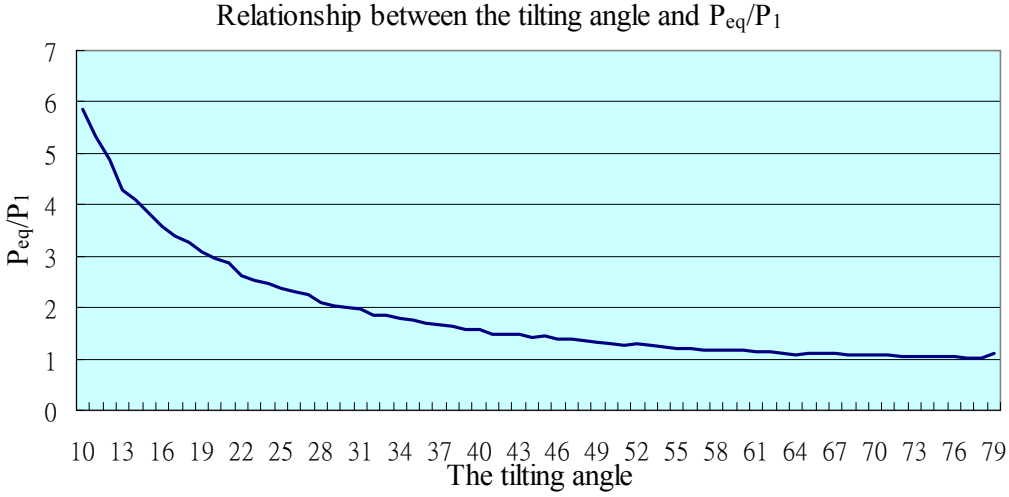

Figure 8. Maximum ratio of the equivalent period with respect to the fringe period 1 determined according to the tilting angle and the fringe period 2 as defined in Fig. 6.

c. Design of band-pass filtering

Most band-pass filters currently employed have a fixed filtering range. This kind of filter is simple but can either lose essential spectral data or include undesired spectral noises in the spectrum domain. Shown in figure 9, the true spectral data region required for accurate surface reconstruction cannot always be acquired using band-pass filtering with a fixed circular range. Thus, it is important to grab as much of the true spectral data region as possible because all the frequency components within the region are essentially required for accurate surface restoration and the redundant spectral data incurring undesired measurement errors should be minimized.

To determine an adequate search range is important for finding the true spectral data region. Shown in figure 10, $f_1(f_{1x}, f_{1y})$ and $f_2(f_{2x}, f_{2y})$, representing the spectral peaks of the fringe pattern 1 and 2, respectively, can be easily identified by finding the spectral peak positions within the corresponding spectral data regions. The radius (f_r) of the searching range can be set as half of the distance between f_1 and f_2 as follows:

$$\left\{ f_r \in Q \mid f_r \le \frac{\overline{f_1 f_2}}{2} \right\} \tag{11}$$

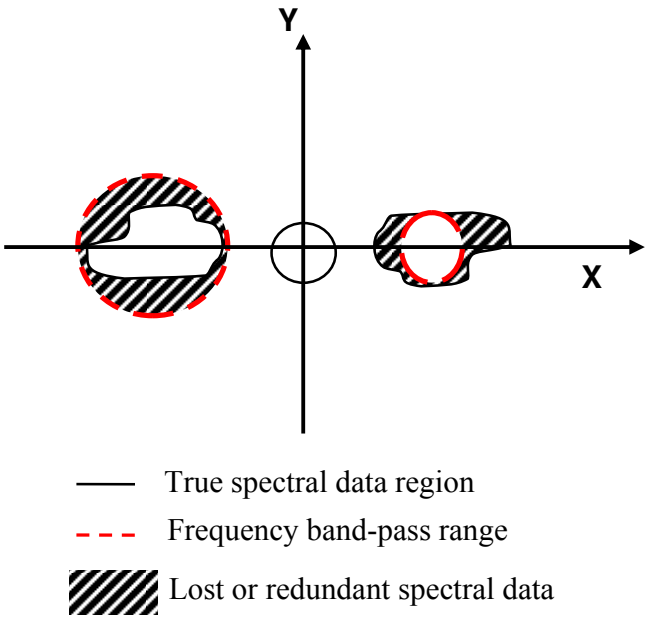

Figure 9. General problems in conventional band-pass filtering strategies, in which the true spectral data region is not accurately selected when using a fixed circular radius.

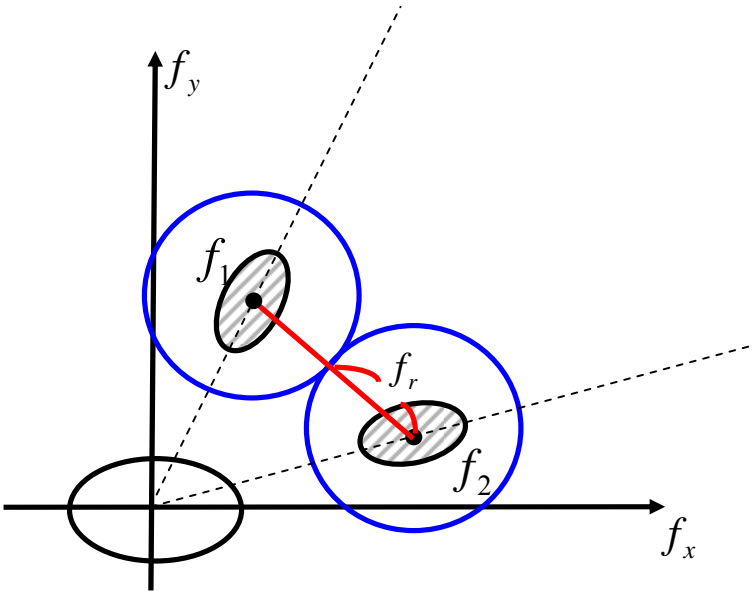

Figure 10. Radius (f_r) of spectral search range can be set as half the distance between f_1 and f_2, representing the spectral peaks of the fringe pattern 1 and 2, respectively.

Meanwhile, shown in figure 11, a threshold value of the spectral data range is defined as $k \cdot h(f_n)_{n=1,2}$ to determine the spectral data region for the fringe pattern 1 (n = 1) and fringe pattern 2 (n = 2) as follows:

$$\begin{cases} T = k \cdot h(f_n)_{n=1,2} \\ h(f) = h(f) & \text{for} \quad h(f) \geq T \\ h(f) = 0 & \text{for} \quad h(f) < T \end{cases} \tag{12}$$

where k is a constant and $k < 1$;

$h(f)$ is the spectral value;

T is the threshold value; and

$h(f_n)_{n=1,2}$ is the peak spectral value.

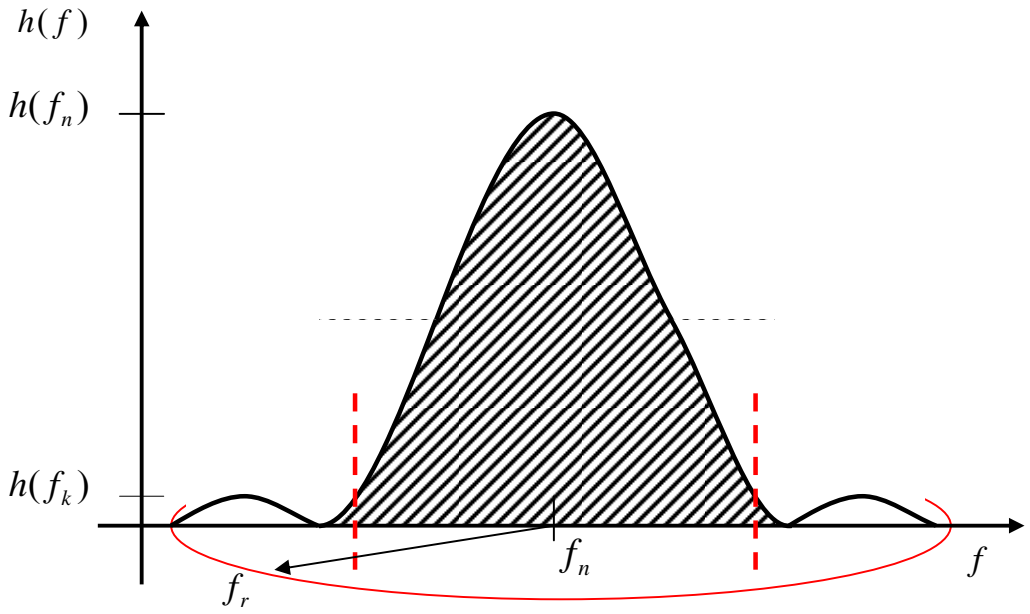

Figure 11. Threshold value of spectral data range defined as $k \cdot h(f_n)_{n=1,2}$ to determine the spectral data region for the fringe pattern 1(n=1) and fringe pattern 2 (n=2).

To obtain precise surface reconstruction, it is important to determine an optimized parameter, k, for ensuring accuracy of profilometry with both dimensional and form restoration quality. In this research, k is determined by a calibration method employing a calibrated standard spherical

(ceramic) ball with a radius of 15.0 ± 0.00025 mm and a ball sphericity of 0.25 μm. The target having an accurate calibrated dimension and spherical reference shape representing a wide variety of surface curvatures covering within a semi-spherical region is measured by the proposed two-frequency fringe pattern method. The optimized k is determined by evaluating the measurement accuracy of the target surface profilometry on both dimensional and form aspects.

d. Phase calculation for 3-D reconstruction

With band-pass filtering, the individual spectral data representing the fringe patterns 1 and 2 can be extracted from the spectrum domain. Two individual phase-wrapped images, $\Delta\phi_1(x, y)$ and $\Delta\phi_2(x, y)$, can be further obtained by applying the inverse fast Fourier transform (IFFT) to the two spectral data 1 and 2 as follows:

$$\Delta\phi_1 = \tan^{-1}\left(\frac{\mathrm{Im}[c_1]}{\mathrm{Re}[c_1]}\right) \tag{13}$$

$$\Delta\phi_2 = \tan^{-1}\left(\frac{\mathrm{Im}[c_2]}{\mathrm{Re}[c_2]}\right) \tag{14}$$

where c_1 and c_2 are the fringe patterns 1 and 2, respectively, after C_1 and C_2 are transformed by IFFT.

In this approach, since the spatial frequency of the fringe pattern 2 is higher than that of the fringe pattern 1, its vertical measurement resolution is also superior to that obtained by the pattern 1. Therefore, $\Delta\phi_2(x, y)$ is employed to reconstruct continuous surface profiles in which the size of step height of any discontinuous surface portion does not exceed $P_2/2$.

Meanwhile, the wrapped phase ($\Delta\phi_{eq}$) of the equivalent pattern can also be determined using the inverse fast Fourier transform (IFFT) on the equivalent spectral data (C_{eq}) and can be further calculated as follows:

$$\Delta\phi_{eq} = \tan^{-1}\left(\frac{\mathrm{Im}[c_{eq}]}{\mathrm{Re}[c_{eq}]}\right) \tag{15}$$

where c_{eq} is the equivalent pattern after C_{eq} is being transformed by IFFT.

By using a general phase unwrapping algorithm, the unwrapped phase $\Delta\phi(x,y)$ (either $\Delta\phi_1(x,y)$, $\Delta\phi_2(x,y)$ or $\Delta\phi_{eq}(x,y)$) can be obtained. With the unwrapped phase, the height of the surface can be defined as [18]:

$$h(x,y)=\frac{l_0\Delta\phi(x,y)}{\Delta\phi(x,y)-2\pi f_0 d} \tag{16}$$

where d is the distance between projector and CCD camera;

l_0 is the distance from CCD camera to reference plane;

P_0, $f_0\left(=1/P_0\right)$ are the fundamental period and frequency of the observed fringe image, respectively.

Assuming that $2\pi f_0 d >> \Delta\phi$, $h(x,y)$ can be further simplified as a linear relationship between the phase difference and the height variation as follows:

$$h(x,y) \approx -\frac{l_0}{2\pi f_0 d}\Delta\phi(x,y)=-\frac{l_0 P_0}{2\pi d}\Delta\phi(x,y) \tag{17}$$

When the two fringe frequencies, f_2 and f_{eq}, are applied in the above equation, respectively, the height of the object surface with respect to the reference plane can be expressed:

$$\begin{aligned} h_{c2}(x,y)&=-\frac{l_0 P_2}{2\pi d}\Delta\phi_2(x,y) \quad \text{if } \Delta\phi_2 \text{ is applied;}\\ h_{eq}(x,y)&=-\frac{l_0 P_{eq}}{2\pi d}\Delta\phi_{eq}(x,y) \quad \text{if } \Delta\phi_{eq} \text{ is applied;} \end{aligned} \tag{18}$$

Either equation from the above can be applied to determine the height, where $h_{c_2}(x,y)$ should be equal to $h_{eq}(x,y)$ theoretically. However, due to the different vertical measurement resolution obtained from using the fringe pattern 2 and the equivalent pattern, the measured heights may deviate slightly from each other. The step height difference between any two adjacent pixels within the field of view can be determined as:

$$\Delta h = h_{n+1}-h_n = -\frac{l_0 P_o}{d}\frac{(\Delta\phi_{n+1}-\Delta\phi_n)}{2\pi} \tag{19}$$

where h_{n+1} is the height located on the pixel of $n+1$;

h_n is the height located on the pixel of n;

$\Delta\phi_{n+1}$ is the phase difference on the pixel of $n+1$; and

$\Delta\phi_n$ is the phase difference on the pixel of n.

Assuming $P_2 < P_1$ in the measurement, for any profile section without having a step height (Δh) between two neighboring pixels exceeding the value of $P_2 l_0 / d$, the fringe period P_2 can be employed to achieve a higher vertical resolution in the developed method. Meanwhile, since P_{eq} is generally larger than P_2, the measurable step height of a phase-discontinuous point can be effectively enhanced by a ratio of $\frac{P_{eq}}{P_2}$ when the step height of any two neighboring points is between $\frac{P_2 l_0}{d}$ and $\frac{P_{eq} l_0}{d}$. Thus, the height of 3-D profile can be determined by combining the unwrapped phases of $\Delta\phi_2$ and $\Delta\phi_{eq}$, which vary with the difference in height between any adjacent pixels, as follows:

$$\begin{cases} h = h_{C2} & for \quad 0 \le |\Delta h| < \frac{P_2 l_0}{d} \\ h = h_{Ceq} & for \quad \frac{P_2 l_0}{d} \le |\Delta h| < \frac{P_{eq} l_0}{d} \end{cases} \tag{20}$$

where h is the calculated height of the object surface.

IV. OPTICAL SYSTEM DESIGN

The optical system layout of the developed methodology is shown in figure 12. The system consists of a digital light projector (DLP) having a 1024 × 768 pixel resolution for generating two-frequency fringe pattern, a CCD with a high speed of up to 200 fps, a personal computer for controlling the projector and acquiring the images through a suitable frame grabber and a set of optical lenses for obtaining the desired characteristics of the fringe pattern. For the optics design, the two-frequency pattern is first projected through a plano-convex (PC) lens to reduce the size of the fringe pattern. Then it passes through a neutral density (ND) filter onto the fringe pattern for optimal intensity control and best image contrast. The pattern is further projected through two double-convex (DC) lenses for pattern size control and light collimation. The size of the fringe pattern projected onto the object can be flexibly adjusted according to the desired measurement specifications and it can be adjusted to suit a variety of inspection tasks. A series of fringe-modulated images of the object can be rapidly captured by the CCD.

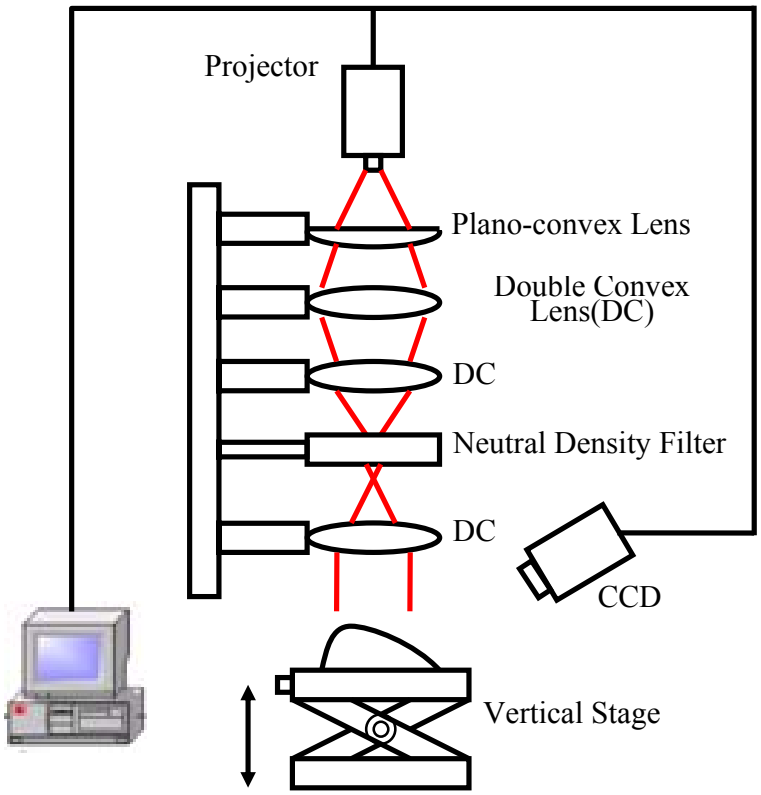

(a)

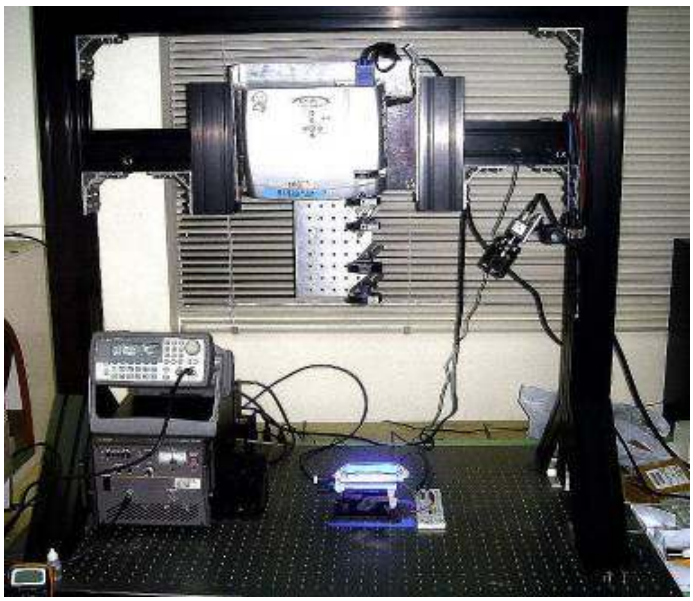

(b)

Figure 12. Optical system layout of the developed methodology: (a) Conceptual diagram and (b) Hardware setup.

In general, vibratory or dynamic motion of the measured object is destructive to the contrast quality of conventional interferometric fringe images. To avoid this, stroboscopic source illumination and signal synchronization are essentially required for capturing a good contrast image in FTP. In the developed system, the stroboscopic imaging system comprises a central control unit, a synchronous control unit, a light-emitting unit and an image-acquiring unit. The central control unit is coupled to the synchronous control unit and the image-acquiring unit. The central control unit controls the synchronous control unit and the image-acquiring unit by its embedded software. The synchronous control unit comprises a wave-form generator and a synchronous controller. Upon receiving a request from the central unit, the wave-form generator generates the control signal. A light-emitting device is coupled to the synchronous control unit and generates a stroboscopic flash upon receiving the control signal. To achieve synchronous image acquisition, the image-acquiring unit is coupled to the central control unit. Upon receiving the control signal, the unit acquires deformed fringe images from the object surface and transmits the images acquired to the central control unit for the phase wrapping and unwrapping processes.

V. EXPERIMENT RESULTS AND DISCUSSION

a. System calibration

Owing to possible image aberration in the measurement, the relationship between the unwrapped phase difference (ϕ) and the object height (H) may show nonlinear variation. To achieve accurate surface reconstruction, a system calibration was performed to analyze the linearity using a series of standard step heights (ranging from 2.0 mm to 9.0 mm) stacked from a group of precision gauge blocks. A least-squares optimization method was employed to identify a mapping model between the unwrapped phase and the object height for the developed measurement system as follows:

$$H = 0.000432\phi^3 - 0.1508\phi^2 + 24.488\phi - 9.398 \quad (21)$$

The maximum and averaged deviations of the above mapping were 152.1 and 34.6 μm, respectively, while the standard deviation of the measurement was maintained within 15.3 μm. The possible maximum error due to the nonlinearity of the measurement system was controlled within 3.3 % of the overall measured height range. The measurement results of the system

calibration can be shown in figure 13. From the calibration results, it is found that the order number (n) used in the least squares fitting algorithm affects the accuracy of the conversion. The fitted error is converged when n is increased up to 3, but it tends to converge to a certain range when an order higher than 3 is applied. Meanwhile, it should be noted that higher order fitting could bring instability to the conversion.

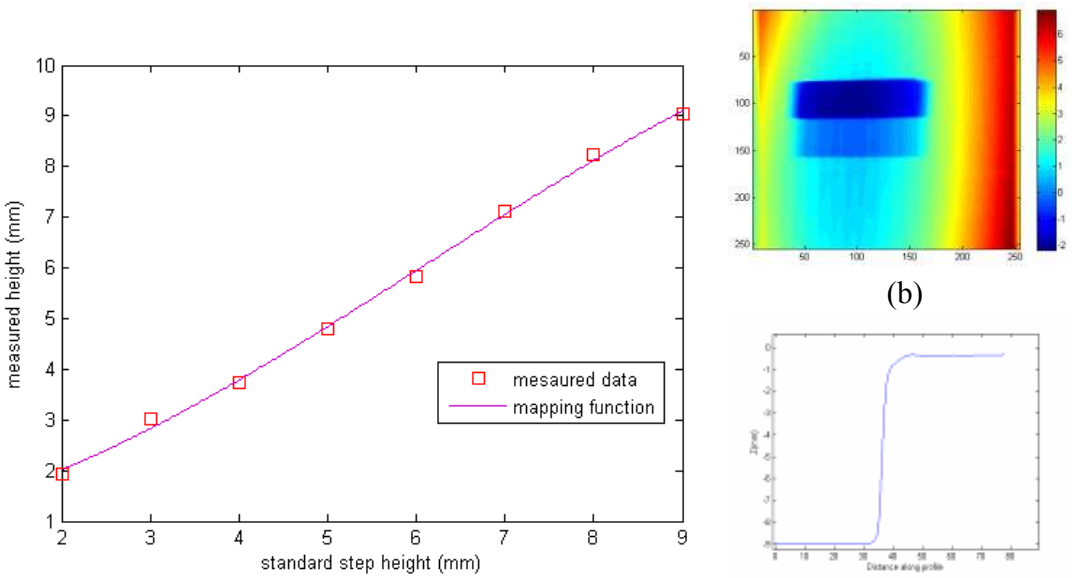

Figure 13. Results of system calibration: (a) the relationship between the measured height and the standard step height; (b) the top view of the measured results; and (c) the profile of one of the measured step heights.

b. Determination of constant parameter k

A calibrated standard spherical ball having a radius of 15.0 ± 0.00025 mm and a ball sphericity of 0.25 μm was employed as a reference target in the proposed method to determine the optimized parameter k. The tilting angle θ between the fringe patterns 1 and 2 was set at four different levels of 15°, 20°, 25° and 30°, respectively. By measuring the calibrated target with the developed two-frequency fringe pattern approach, the dimensional and sphericity measurement errors with respect to the parameter, k, can be obtained and shown in figures 14 and 15, respectively. Analysis of the experimental results reveals that both of the measurement errors converged to a minimum (420 μm for dimension measurement and 7.5 μm for sphericity

measurement when k is set to be 0.1). It was also found that a 20°-tilting angle can provide a feasible solution for achieving a maximum equivalent period of the moiré pattern up to approximately three folds that of the fringe period 1. A higher equivalent period of the moiré pattern can be further enhanced by improving the image quality index (such as MTF) of the optical system, for allowing a finer pitch of the fringe pattern 1 to be employed in the approach.

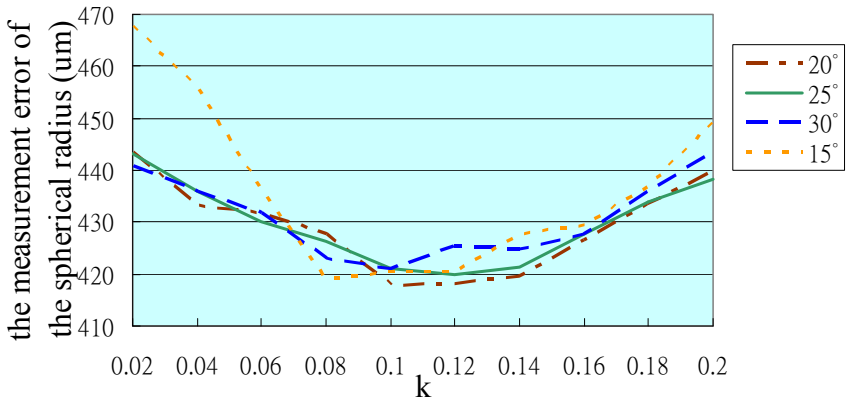

Figure 14. Relationship between k and measured dimensional errors

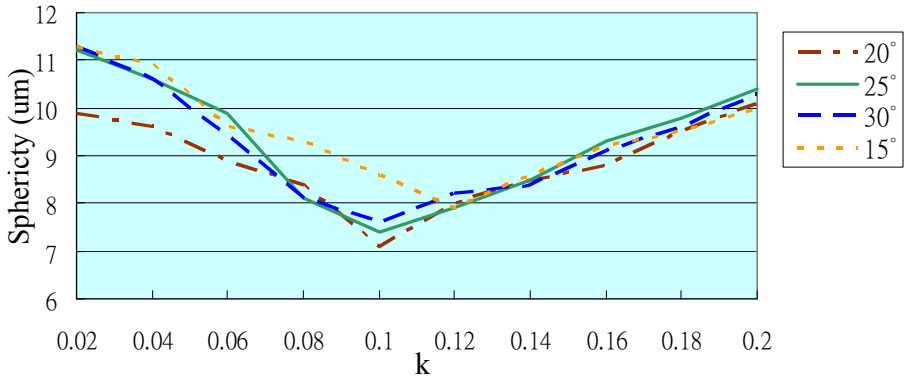

Figure 15. Relationship between k and measured sphericity

c. Analysis on measurement performance of the developed FTP

To analyze its efficiency and precision, the developed FTP approach was compared with the general five-step phase shifting method using the developed DMD-based fringe projection system. Standard step heights of 2.0 ± 0.001 mm and 4.0 ± 0.001 mm (shown in figure 16) obtained by

stacking two precision gauge blocks of ceramic type were employed to evaluate the accuracy of the measurement. In the phase shifting measurement, the period of the single fringe was set at 5.0 mm and the ratio of l_0 / d at 0.66667 in the experiment setup. A series of five phase-shifting deformed images were captured for a general phase wrapping and unwrapping processes. The measurement was performed in a PC with an AMD CPU of 2.08G and 212 MB RAM. The measurement result of the 3-D profile of the tested step height is shown in figure 17, in which the averaged measurement error of the height was 49 μm representing 2.45% of the overall measurement range and the time required for image acquisition and implementing the phase-shift algorithm were 0.14 and 1.59 seconds, respectively. However, the experimental results show that the phase-shifting method failed in measuring the step height of 4.0 mm since it exceeded the measurable step-height detection limit, which is equivalent to 3.333 mm ($= \mathrm{P} l_0 / d$).

For the developed FTP approach using a single fringe projection, the period of the single fringe was 5.0 mm (shown in figure 18(a)) and its spectral peak was located at $f(123,105)$ (shown in figures 18(b) and (c)). The ratio of l_0 / d was kept the same as the one used in the above phase shifting method. By using the band-pass filtering strategy and FTP developed in the approach, the 3-D profile measurement was obtained using the same hardware setup. Analysis of the experimental results indicates that the averaged measurement error of the height was 64 μm representing 3.2% of the overall vertical range and the time spent on image acquisition and implementation of FTP using a single fringe projection was 0.03 and 1.98 seconds, respectively. The measurement accuracy of the single fringe FTP was slightly less than the one obtained by the phase shifting method. However, the image acquisition time required by the one-shot FTP method was only approximately 20 % of the one required by the phase shifting method. This advantage significantly reduces potential risks in suffering image noises coming from the environmental disturbances (mainly from vibrations) since the deformed fringe can be acquired in a much short period of time. Meanwhile, the phase shifting errors severely encountered by many phase shifting methods can be avoided by the proposed FTP method. However, due to lengthy time required in the fringe phase computation (especially in the current software operation of Fast Fourier Transform (FFT) and Inverse FFT) the overall time spent for the developed FTP is slightly larger than the one required for the phase shifting method. Fortunately, the phase analysis required by the FTP does not affect the anti-vibration capability of the one-

shot FTP and its computation efficiency can be further improved by advanced high-speed FFT hardware solution or parallel processing strategies.

It is worth noting that the FTP method using single fringe projection is also failed in reconstructing the step height of 4.0 mm since it exceeds the detection limit of Pl_0 / d. In addition, shown in figures 18 (d) and (e), it indicates that the step height of the reconstructed 3-D map tends to lose the step-height shape edges. This problem could be attributed to the loss of higher spectral data representing the sharp geometric feature of the measured surface in the band-pass filtering process. This issue can be further investigated and improved in the near future research.

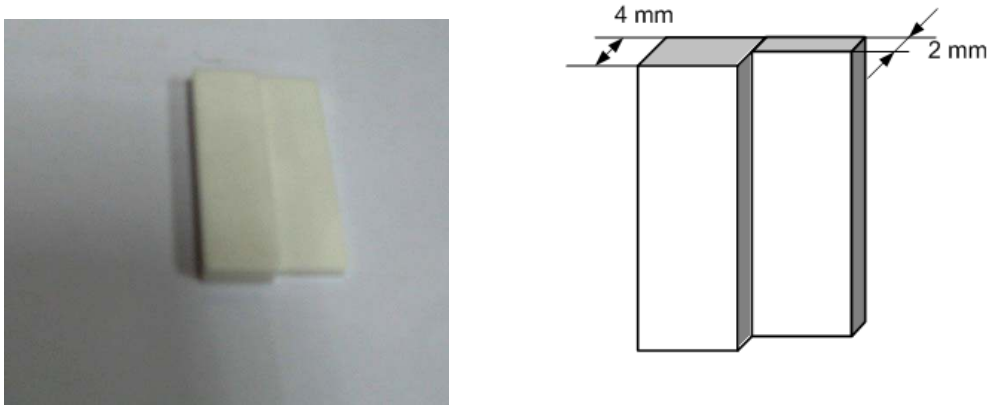

(a) (b)

Figure 16. Standard step heights of 2 mm and 4 mm obtained from overlapping two precision gauge blocks for testing measurement accuracy.

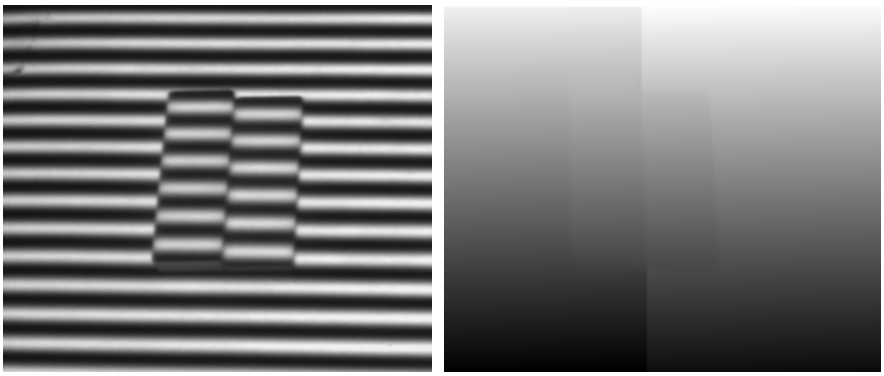

(a) (b)

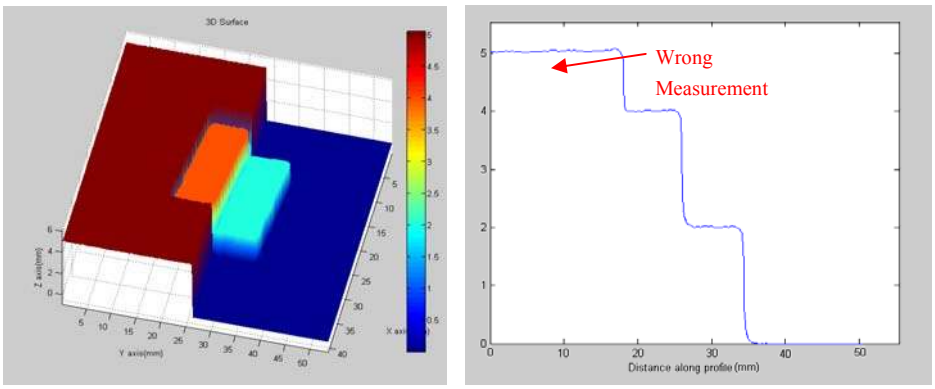

(c) (d)

Figure 17. Result of 3-D profile of tested step height measured using the general five-step phase shifting method and the developed DMD-based fringe projection system: (a) the deformed fringe image; (b) the unwrapped phase map; (c) the 3-D map of the reconstructed surface; and (d) the y-axis cross-section profile of the reconstructed surface.

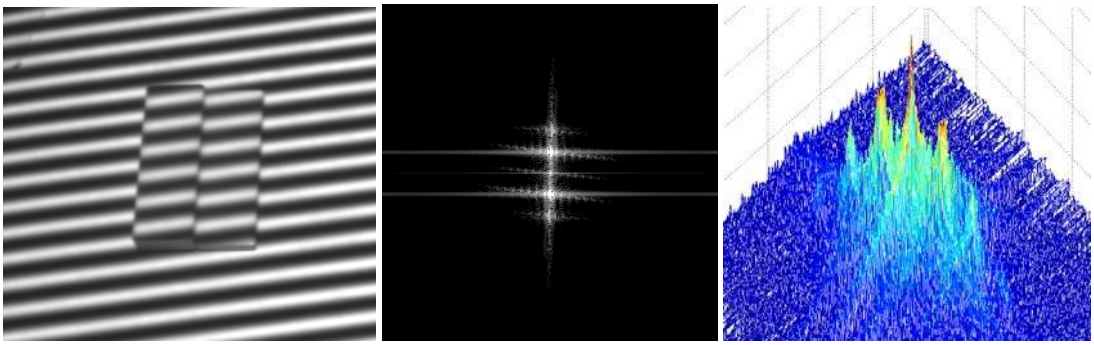

(a) (b) (c)

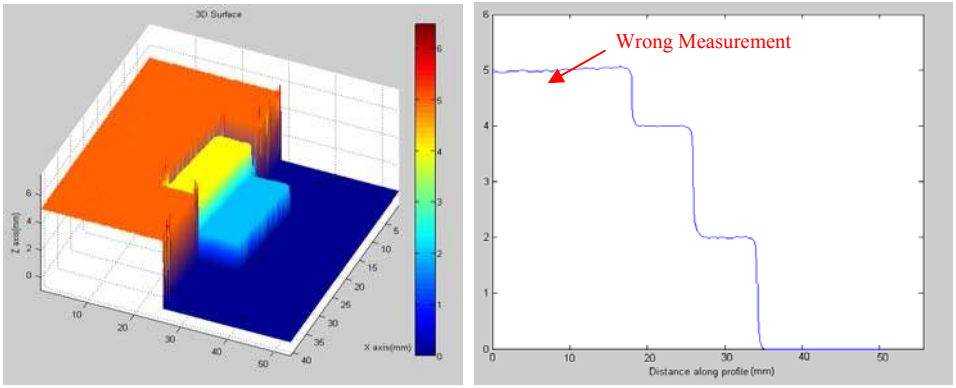

(d) (e)

Figure 18. Result of 3-D profile of tested step height measured using the developed FTP approach with a single-frequency fringe pattern projection: (a) the deformed fringe image; (b) the top view of the spectrum data; (c) the 3-D view of the spectrum data; (d) the 3-D map of the reconstructed surface; and (e) the y-axis cross-section profile of the reconstructed surface.

For the developed FTP approach using a two-frequency pattern projection, the period of both fringe patterns 1 and 2 was 5.0 mm and a tilting angle of 20° was employed, in which an equivalent period P_{eq} of 14.4 mm was formed. The ratio of l_0 / d was kept the same as the previous experiments. The deformed fringe image of the projected two-frequency moiré pattern is shown in figure 19(a) and its three spectral peaks of C_1, C_2 and C_{eq} were located at $p_1(123,105)$, $p_2(120,109)$ and $p_{eq}(135,127)$, respectively, whose top and 3-D view are shown in figures 19(b) and 19(c), respectively. With a searching radius (f_r) of 7.071 and the threshold parameter (k) of 0.1, the individual boundaries of the spectral 1, spectral 2 and equivalent spectral data regions were detected. With the developed approach, the 3-D and 2-D profile of the measured height can be obtained and are shown in figures 19(d) and 19(e), respectively. Analysis of the experimental results suggests that the averaged measurement error of the height was 66 μm representing 3.31% of the overall measurement range and the time spent on image acquisition and implementation of FTP using a two-frequency fringe pattern projection was 0.03 and 2.6 seconds, respectively. The performance of the two-frequency moiré FTP method was similar to the one of the single frequency FTP except its overall time spent is longer. This could be mainly induced by its intensive processing required in the fringe analysis. However, the measurement results of the step height of 4.0 mm shown in figures 19 (d) and (e) clearly demonstrate that the method is capable in reconstructing the step height of 4.0 mm. This can be well explained by the fact that the measurable step-height detection limit has been extended to 9.6 mm in the two-frequency moiré FTP. Moreover, the crucial time duration required for image acquisition was still kept as the same with the single frequency moiré method. This indicates that the anti-vibration capability of the two-frequency moiré FTP being developed is the same with the one of the single frequency method.

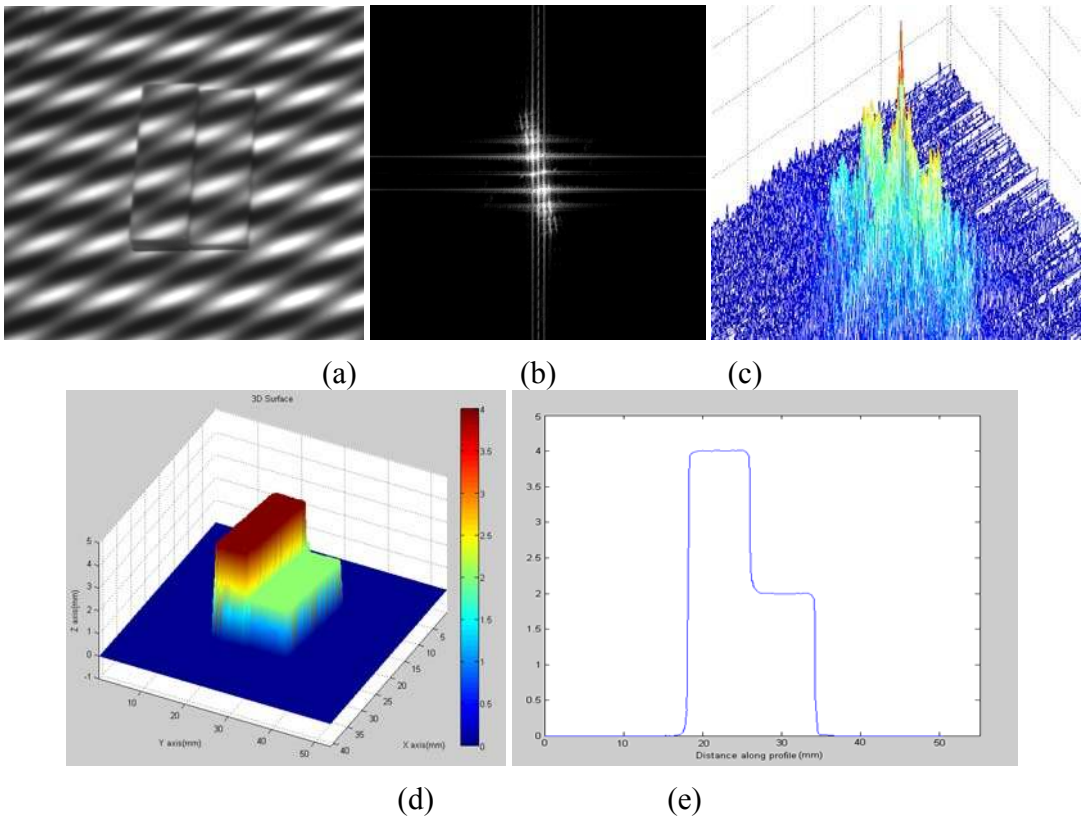

Figure 19. Result of 3-D profile of tested step height measured using the developed FTP approach with a two-frequency moiré fringe projection: (a) the deformed fringe image; (b) the top view of the spectrum data; (c) the 3-D view of the spectrum data; (d) the 3-D map of the reconstructed surface; and (e) the y-axis cross-section profile of the reconstructed surface

Analyzing the measurement performance of the above three methods reveals that the proposed two-frequency moiré fringe FTP method prevails over the other two methods. Although the phase shifting (PS) method is slightly more accurate than that achieved by the FTP method, it is difficult to be applied for real-time measurement of vibrating objects since its image acquisition time is too lengthy to acquire accurate phase-shifted images without having disturbances from the environmental noises. The FTP method is excellent in having a short image capturing time, thus achieving better resistance to vibration disturbance. In addition, the proposed two-frequency moiré fringe FTP method has a higher measurable step-height range for reconstructing arbitrary surfaces. The DMD-based measurement approach developed has its exclusive advantage of achieving flexibility in optimizing the fringe pattern for ensuring its effectiveness in

reconstructing 3-D surfaces. Furthermore, it is also confirmed that the developed FTP method could require high-speed hardware or parallel processing strategies to shorten the time spent in its intensive FFT operation.

d. Measurement of vibratory membrane of a sound speaker

The vibratory membrane of a planar three-layer sound speaker of composite type shown in figure 20 was measured by the developed FTP approach as its feasibility test on dynamic measurement. The tested object has a mean reference of curvature of 99.0 mm long, and is 36.0 mm wide and 2.2 mm thick. A two-frequency moiré fringe with setup parameters of P_1 at 5 mm, P_2 at 5 mm and θ at 20° was projected onto the vibratory membrane, thus achieving an equivalent fringe period (P_{eq}) of 14.4 mm. The vibration excitation frequency of the tested object was set to be 30 Hz and the input voltage of the sinusoidal single was set to be 7.0 volts. Stroboscopic source illumination and signal synchronization were employed to ensure good-contrast deformed fringe images captured by the approach. By using the developed methodology, the deformed fringe (shown in figure 21(a)) of the projected two-frequency moiré pattern was transformed to the spectrum domain shown in figures 21(b) and (c) for different views. The spectral peak of C_1, C_2 and C_{eq} were located at $p_1(120,106)$, $p_2(127,105)$ and $p_{eq}(135,127)$, respectively, as shown in figure 21(c). Figures 21(d) and (e) illustrate the wrapped and unwrapped phase map of the surface reconstructed using the developed FTP methodology when the tested object was vibrated at a particular position. Since the current processing time required by the FTP method could be too lengthy, a series of deformed fringe images were first acquired in its real-time behavior and then processed by the developed measurement method in an off-line data processing stage. The dynamic motion and behavior of the tested membrane can be obtained and analyzed (shown in figure 22). The tested object was vibrating with a linear vertical motion at a vibratory amplitude of 1.910 mm. The 3-D vibratory mode shape and dynamic characteristics of the object can be analyzed effectively.

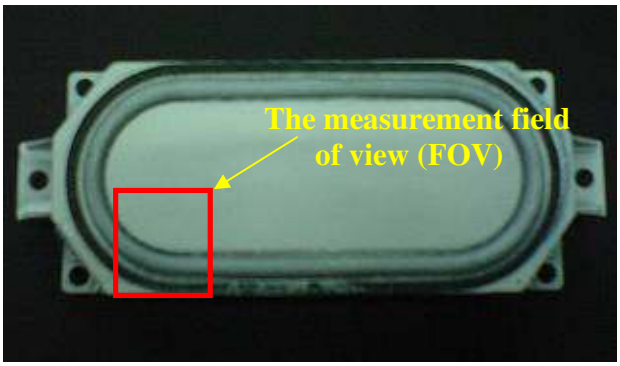

Figure 20. Vibratory membrane of a planar three-layer sound speaker of composite type measured by the developed FTP approach.

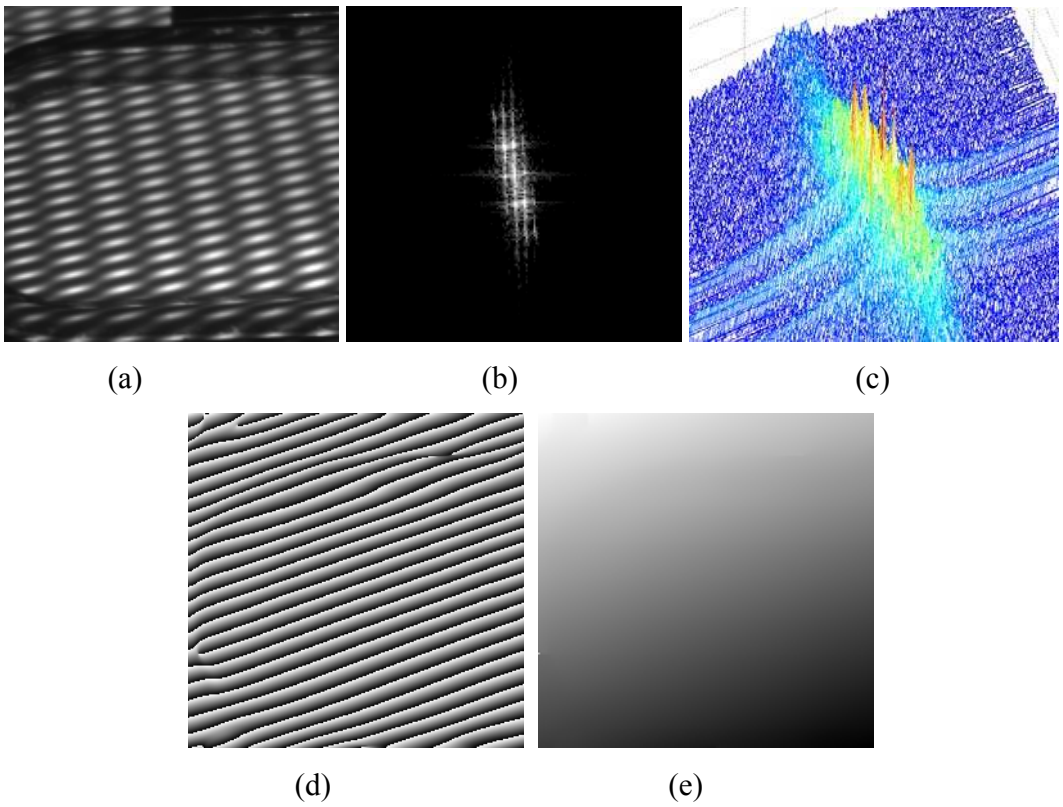

Figure 21. Result of dynamic 3-D profile reconstruction of the tested vibratory membrane measured using the developed FTP approach with a two-frequency moiré fringe projection: (a) the deformed fringe image; (b) the top view of the spectrum data; (c) the 3-D view of the

spectrum data; (d) the wrapped phase map; and (e) the unwrapped phase map of the reconstructed surface.

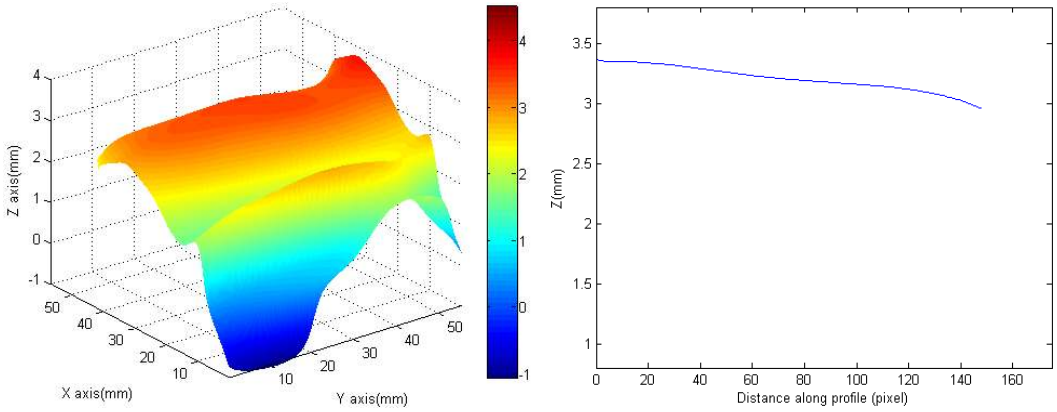

(a)

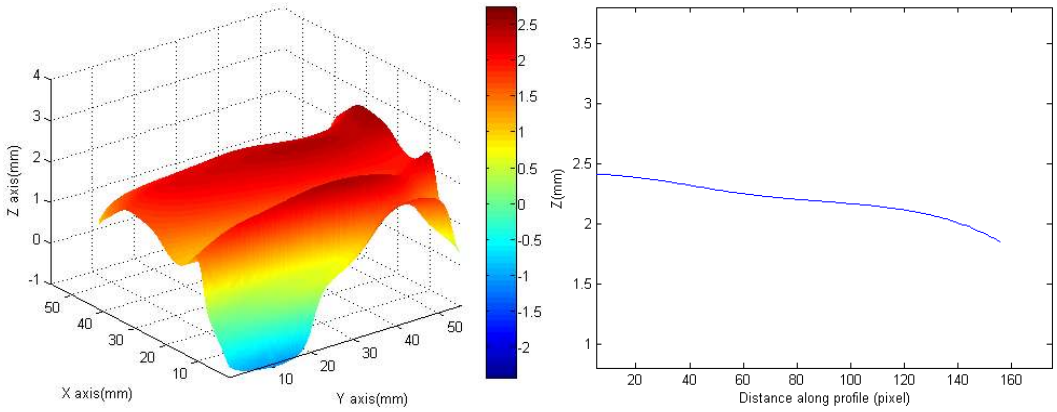

(b)

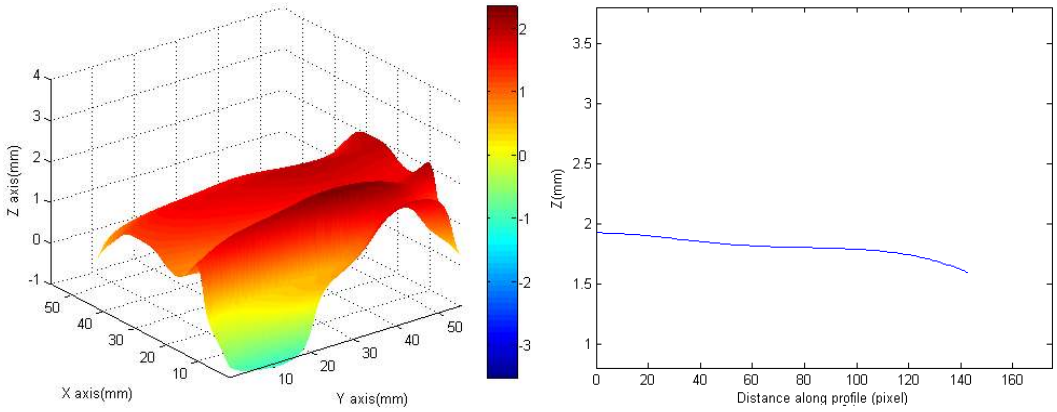

(c)

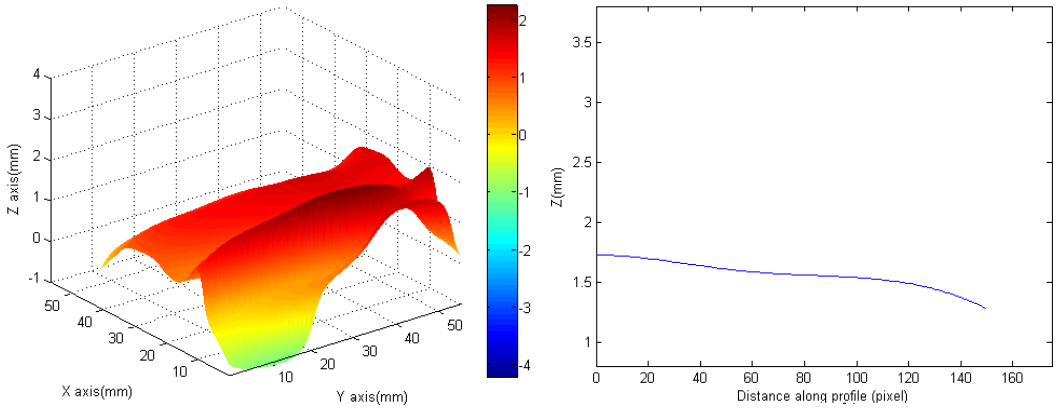

(d)

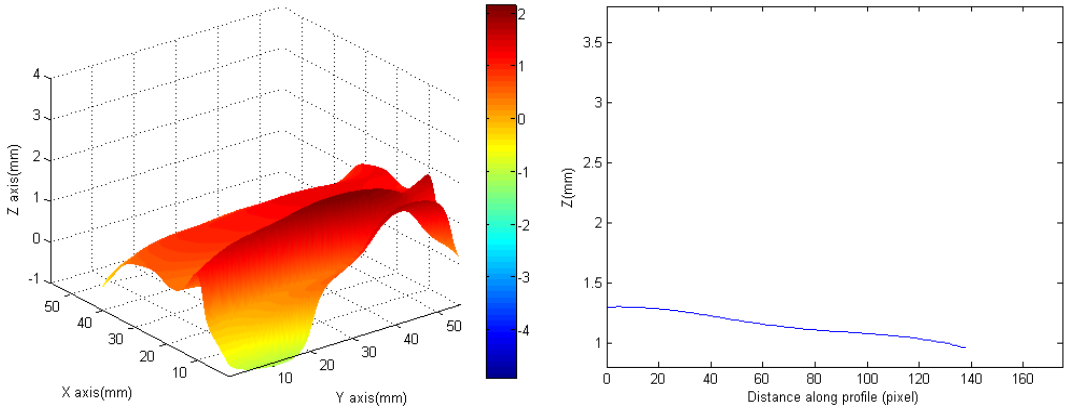

(e)

Figure 22. Dynamic measurement results of the tested vibratory membrane under different vibrating duration: (a) T_1=1/30 sec; (b) T_2=5/30 sec; (c) T_3=9/30 sec; (d) T_4=13/30 sec; and (e) T_4=17/30 sec.

VI. CONCLUSIONS

In this article, a novel two-frequency moiré pattern projection using FTP was developed to achieve one-shot image 3-D surface profilometry. The measurement speed can be significantly increased, thus avoiding problems due to potential in-field vibration. In this research, an innovative moiré design method and an effective band-pass filtering strategy were developed to separate the important spectral data regions for ensuring accurate surface reconstruction. A calibration approach was effectively developed to determine the spectral data boundary for enhancing dimensional measurement accuracy as well as geometric form restoration. The DMD-

based two-frequency moiré pattern FTP can be employed to increase the measurable step-height range while maintaining the measurement accuracy at the same level achieved using single-frequency pattern projection. The experimental results preliminarily verified that the maximum measured error using the developed method can be controlled within 3.5% of the overall measuring depth range. To further achieve a real-time 3-D measurement, advanced high-speed FFT hardware solution as well as a more effective band-pass filter for reconstructing sharp geometric feature is required in the future development.

ACKNOWLEDGEMENT

The authors would like to thank the National Science Council of Taiwan, for financially supporting this research under Grant NSC 95-2221-E-027-084.

REFERENCES

[1] T. L. Pennington, H. Xiao, R. May and A. Wang, “Miniaturized 3-D surface profilometer using a fiber optic coupler”, Opt. Laser Technol, Vol. 33, 2001, pp. 313-320.

[2] L. C. Chen and C. C. Huang, “Miniaturized 3D surface profilometer using digital fringe projection”, Meas. Sci. Technol, Vol. 16, 2005, pp. 1061-1068.

[3] L. C. Chen and Y. W. Chang, “Development of Simultaneous Confocal Full-Field Surface Profilometry for Automatic Optical Inspection (AOI)”, The 35th international MATADOR conference (Taiwan), Vol. 35, 2007, pp. 237-240.

[4] G. Sansoni, L. Biancardio, U. Minoni and F. A. Docchio, “Adaptive system for 3-D optical profilometry using a liquid crystal light projector”, IEEE Trans. Instrum. Meas., Vol. 43, 1994, pp. 558-566.

[5] L. C. Chen and C. C. Liao, Mater. Sci. Forum, Vol. 16, 2005, pp. 1554-1566.

[6] S. Zhang and S. T. Yau. “High-resolution, real-time 3D absolute coordinate measurement based on a phase-shifting method”, Opt. Exp., Vol. 14, 2006, pp. 9120-9129.

[7] O. Ribun and I. Yukihiro, “Two-Wavelength Interferometry That Uses a Fourier-Transform Method”, Appl. Opt., Vol. 37, 1998, pp. 7988-7994.

[8] W. Chen, X. Su, Y. Cao, L. Xiang and Q. Zhang, “Fourier transform profilometry based on a

fringe pattern with two frequency components", Proc. SPIE, Vol.6027, 2006, pp. 395-403.

[9] A. Shulev, I. Russev and V. Sainov, "New automatic FFT filtration method for phase maps and its application in speckle interferometry", Proc. SPIE, Vol. 4933, 2003, pp. 323-327.

[10] X. Su and Q. Zhang, "Optical 3D shape measurement for vibrating Drumhead", Proc. SPIE, Vol. 6027, 2006, pp. 449-455.

[11] S. Zhang and P. Huang, "High-resolution, real-time 3d shape acquisition", IEEE Computer Vision and Pattern Recognition Workshop on Real time 3D Sensors and Their Uses, Vol. 3, 2004, pp. 28-37.

[12] N. Brock, J. Hayes, B. Kimbrough, J. Millerd, M. North-Morris, M. Novak and J. C. Wyant, "Dynamic interferometry", Proc. SPIE, Vol. 5875, 2005, pp. 58750F1-10.

[13] P. Vuylsteke and A. Oosterlinck, "Range image acquisition with a single binary-encoded light pattern", IEEE T. Pattern Anal., Vol. 12, 1990, pp. 148-163.

[14] P. Griffin, L. Narasimhan and S. Yee, "Generation of uniquely encoded light patterns for range data acquisition", Pattern Recogn., Vol. 25, 1992, pp. 609-616.

[15] O. Hall-Holt and S. Rusinkiewicz, "Stripe boundary codes for real-time structured-light range scanning of moving objects", The 8th IEEE International Conference on Computer Vision, Vol. 8, 2001, pp. 359-366.

[16] M. Takeda and K. Muloh, "Fourier-transform profilometry for the automatic measurement of 3-D object shapes", Appl. Opt., Vol. 22, 1983, pp. 3977-3982.

[17] Y. Arai, S. Yokozeki and K. Shiraki, "Experimental modal analysis for vibration with large amplitude using moiré topography", Proc. SPIE, Vol. 3098, 1997, pp. 176-182.

[18] L. C. Chen, Y. T. Huang and K. C. Fan, "A dynamic 3-D surface profilometer with nano-scale measurement resolution and MHz bandwidth for MEMS characterization", IEEE/ASME Transaction on Mechatronics, Vol. 12, 2007, pp. 299-307.

[19] R. Onodera and Y. Ishii, "Two-Wavelength Interferometry That Uses a Fourier-Transform Method", Appl. Opt., Vol. 37, 1998, pp. 7988-7994.